

Novel Honeycomb-Patterned SMOOTH-Mode Technology for Intense Heat Shock Biomodulation (i-HBM)

Marko Kažič¹, Jure Košir^{1,2}, Boris Cencič¹, Matej Senegačnik¹, Adrian Gaspar⁵, Matjaž Lukač^{1,3,4}

¹Fotona d.o.o., Stegne 7, Ljubljana, Slovenia

²University of Ljubljana, Faculty of Mechanical Engineering, Askerceva 6, Ljubljana, Slovenia

³Institut Josef Stefan, Light and Matter Dept., Jamova 39, Ljubljana, Slovenia

⁴University of Ljubljana, Faculty of Mathematics and Physics, Jadranska 19, Ljubljana, Slovenia

⁵Espacio Gaspar Clinic, Mendoza, Argentina

ABSTRACT

The introduction of a special Er:YAG “FotonaSMOOTH®” modality has made it possible to utilize the Er:YAG laser’s unique absorption characteristics for minimally invasive yet highly effective non-ablative treatments. The clinical outcomes of FotonaSMOOTH® treatments have been substantially enhanced by a special “polka dot” patterned beam (PS03-type) technology.

In this paper, we introduce a novel HC⁶ “HoneyComb™” beam pattern technology that mimics the honeycomb pattern very often observed in nature due to its most spatially-efficient design.

Key words: Er:YAG laser, FotonaSMOOTH, SMOOTH, superficial triggering, i-HBM, Intense heat shock biomodulation

Article: J. LA&HA, Vol. 2023, No.1; onlineFirst.

Received: Nov 10, 2023; Accepted: Dec 18, 2023.

© Laser and Health Academy. All rights reserved.

Printed in Europe. www.laserandhealth.com

I. INTRODUCTION

Due to its extremely high absorption in water ($\delta \approx 1 \mu\text{m}$) the Er:YAG laser therapy has been extensively investigated and employed for various ablative procedures, including skin resurfacing and removal of lesions [1-4].

More recently, the introduction of a special Er:YAG FotonaSMOOTH® modality has made it possible to utilize the unique Er:YAG laser technology for non-ablative treatments as well [5-7]. As opposed to ablative resurfacing, where the epithelium gets ablated, the non-ablative FotonaSMOOTH® laser uses a thermal pulsing approach to induce tissue regeneration without obvious epithelial injury. This non-ablative regeneration modality has enabled a number of minimally invasive yet very effective treatments in aesthetics, and as well in ENT and gynecology [8-25].

The FotonaSMOOTH® mode modality is based on a burst (train) of short micro-pulses comprising an overall super-long SMOOTH macro-pulse (see Fig. 1). Based on this dual-temporal characteristic, FotonaSMOOTH® combines both fast and slow heating of the tissue. First, due to the fast thermal diffusion from the very thin ($\approx 1\text{-}3 \mu\text{m}$) heated superficial tissue layer, the duration of the thermal exposure to short micro pulses and to resulting high temperature peaks (T_{max-i}) is extremely short ($t_{exp-i} < 1$ ms). On the other hand, the duration of the long-duration temperature T_{max} , representing the long-duration temperature exposure to the overall SMOOTH mode energy delivery, is longer, resulting in the long-duration temperature exposure time (t_{exp}) of up to several seconds.

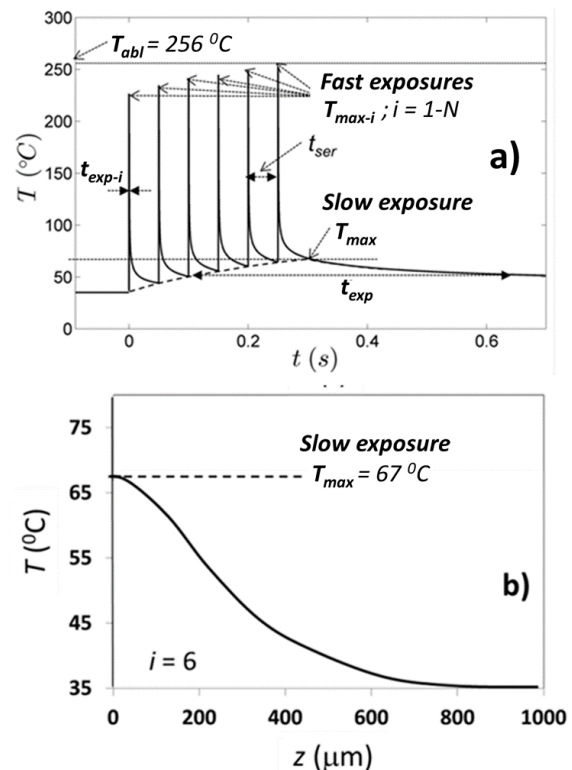


Fig. 1: FotonaSMOOTH® mode Er:YAG laser pulse sequence (an example for $N = 6$ is shown) and resulting temperatures for an exemplary laser setting [7].

The importance of the difference in the cooling times

for the two modes of thermal exposure during the SMOOTH irradiation can be best appreciated by considering that the thermal damage kinetics during laser procedures is commonly described by the Arrhenius damage integral [26-28], and that according to the VHS (Variable Heat Shock) Arrhenius' model, the critical temperature (T_{crit}) for irreversible tissue damage is relatively low ($T_{crit} \approx 45-65$ °C) for long thermal exposures t_{exp} , and significantly higher ($T_{crit} > 250$ °C) for extremely short-duration exposures t_{exp-i} [28].

Despite the technique's "smoothness" the regenerative response of the tissue to FotonaSMOOTH® treatments is substantial [5-25]. This is because the dual-heat delivery of the non-ablative Er:YAG SMOOTH mode irradiation produces two very distinct types of tissue reactions at different tissue depths (see Fig. 2) [6, 25, 28]:

- Intense Heat-Shock Biomodulation (i-HBM): high peak temperatures (T_{max-i} up to ≈ 250 °C) within the thin superficial tissue layer that last for a very short time (FAST exposure);
- Deep (see Fig. 1b) hyperthermia/coagulation: lower levels of gradually increasing deeper heat deposition with a longer exposure time (SLOW exposure).

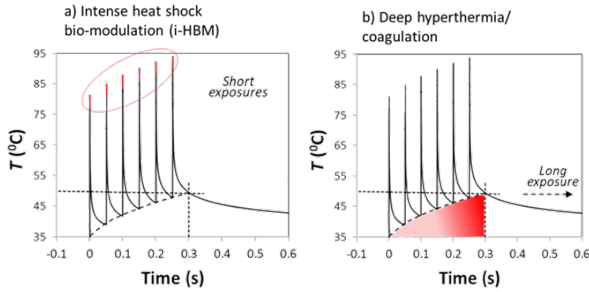


Fig. 2: The FotonaSMOOTH® dual heat delivery.

The conventional approach for tissue regeneration focuses on a slow heating of the connective tissue, in order to stimulate fibroblasts and other cells to respond to wound healing scenarios [25, 53]. In contrast, the FotonaSMOOTH® approach is based on an indirect mechanism whereby the keratinocytes and other cells located in the superficial layer above the basement membrane are activated (i.e., triggered) by extremely fast and intense "heat shock" thermal pulses. The intense heat shock biomodulation (i-HBM) is generated by intense, very short thermal pulses of up to ~ 250 °C that create a superficial heat-shock event without exceeding the critical temperature for tissue damage [25, 28]. This stress generates a cascade of inter-cellular communication that carries alarm signals triggering the body's bio-modulative repair mechanisms, including

fibroblast proliferation, increased collagen, and vascularization deeper within the tissue.

The contribution of i-HBM to the total FotonaSMOOTH®-induced dual-regeneration process has been recently evaluated by comparing treatment efficacies of three FotonaSMOOTH® biomodulation protocols in terms of the number of generated positive fibroblasts per delivered laser fluence [29]. Figure 3 shows the results of this in-vivo immune-histology study for protocols designed to generate either predominantly i-HBM or predominantly hyperthermic biomodulation, and for a protocol combining both the i-HBM and hyperthermic biomodulation effect. Results show that the i-HBM contributes substantially to the tissue regeneration, and that combining the i-HBM and hyperthermic biomodulation mechanisms results in a significant synergistic enhancement of tissue regeneration.

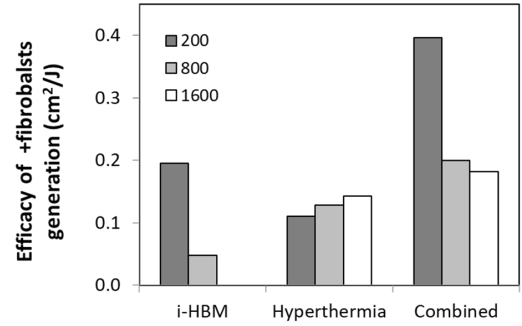


Fig. 3. Comparison of treatment efficacies of three FotonaSMOOTH® biomodulation protocols, in terms of the number of generated positive fibroblasts per delivered laser fluence, for skin depths of 200 μm , 800 μm and 1600 μm [29].

Ignoring patients' discomfort, the level of i-HBM triggering can be increased by increasing the fluence (F_i) and/or the number (N) of delivered micro pulses. Measurements have shown that the pain threshold depends mainly on the long-exposure skin temperature T_{max} at the end of the FotonaSMOOTH® pulse sequence, and not on the peak skin temperatures (T_{max-i}) following individual laser pulses within the sequence [7]. Since the final base-line temperature (T_{max}) depends on the total delivered laser fluence $F = \sum F_i$, and T_{max} is required to be below the pain threshold (determined to be at $\sim 47-48$ °C without topical anesthesia, and at $\sim 51-52$ °C with topical anesthesia) [7], this requirement puts a limit on the maximally allowed fluence and number of individual laser micro pulses, and therefore also on the maximally achievable level of superficial heat-shock triggering (i-HBM).

In addition to the delivered fluence, the final base-line temperature depends also on how much the heated tissue surface cools down in-between micro pulses. An obvious way of increasing the effect of i-HBM without

exceeding the pain threshold is therefore to reduce the pulse repetition rate by extending the time t_{ser} (see Fig. 1) in-between the micro pulses (see Fig. 1). This is why the V-SMOOTH scanner variant of the FotonaSMOOTH® modality allows the operator to conveniently adjust the duration of the 6-pulse SMOOTH train from 125 to 625 ms.

However, a substantial further enhancement of the i-HBM effect can be achieved by increasing the rate of tissue cooling. With this goal, special handpieces with a unique “polka dot” patterned beam have been developed, wherein the laser beam irradiates a number of individual circular spots within the overall treatment area [7, 10]. Patterned handpieces allow cooling of the irradiated tissue not only by the heat diffusion deeper into the tissue but also by the heat diffusion in a radial direction away from the irradiated micro-spots, thus increasing the range of the achievable i-HBM effect.

In this paper, we introduce a novel “honeycomb” beam pattern technology as an alternative means for enhancing the FotonaSMOOTH® generated i-HBM tissue regeneration process.

II. MATERIALS AND METHODS

a) Apparatus

The Er:YAG system used was a Dynamis SP (manufactured by Fotona, d.o.o. Slovenia). The laser was flashlamp pumped and was fitted with a non-contact scanning handpiece Fotona T-Runner. The laser was operated in the scanning V-SMOOTH variant of the FotonaSMOOTH® modality, with the adjustable SMOOTH mode pulse duration $t_{SMOOTH} = 125\text{-}650$ ms.

Abdominal skin temperatures were measured using a thermal video camera ThermaCAM P45 (manufactured by FLIR Systems, USA).

b) FotonaSMOOTH® modality

The FotonaSMOOTH® technology delivers Er:YAG optical laser energy in a stack (N_{stack}) of SMOOTH mode pulses (see Fig. 4). The SMOOTH mode pulse consists of six temporally spaced, micro laser pulses ($t_i \approx 0.3\text{-}0.45$ ms) within an over-all adjustable duration of $t_{SMOOTH} = 125\text{-}650$ ms. The structure of the SMOOTH mode is designed to prevent temperature build-up at the surface, and to achieve homogenous heating within a several-hundred-microns thick superficial layer of the treated tissue. The cumulative fluence ($F = \sum F_i$; in J/cm^2) and the duration $t_{SMOOTH-N}$ of the burst of the adjustable number (N_{STACK}) of SMOOTH macro-pulses, and the repetition rate (f in Hz or s^{-1}) of the burst (i.e., of the SMOOTH macro-pulses) can be set by the practitioner.

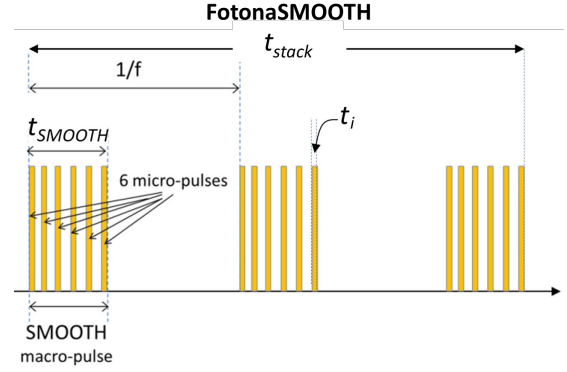


Fig. 4. Temporal structure of the FotonaSMOOTH® modality for $N_{stack} = 3$. The total number of micro-pulses is equal to $N = 6 \times N_{stack} = 18$.

During and immediately following individual laser micro pulses i , it is the rapid longitudinal cooling deeper into the tissue that predominantly determines the thermal exposure time. However, during the time in-between laser pulses, the slower transverse cooling due to the heat diffusion in the radial direction away from a laser irradiated spot may become important as well (see Fig. 5). The transverse cooling effect becomes more pronounced for spot sizes smaller than ~ 1.5 mm (24), where the transverse cooling time of 1.4 s (See Eq. 1) becomes comparable to a typical duration t_{stack} of the FotonaSMOOTH pulse train.

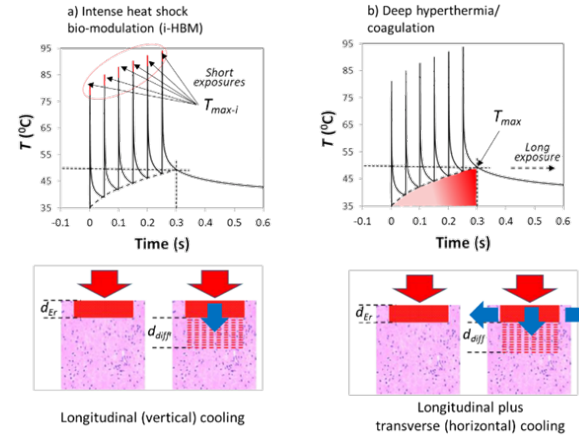


Fig. 5. a) Short-duration (< 1 msec) exposures to T_{max-i} depend predominantly on a fast rate of longitudinal cooling deeper into the tissue; b) Long-exposure duration (seconds) to T_{max} depends on both, the longitudinal cooling and as well on the rate of cooling radially away from the irradiated spot. This transverse cooling effect becomes more pronounced for spot sizes smaller than ~ 1.5 mm .

c) Polka dot beam pattern

When irradiation is performed in a “full-spot” manner a typical laser spot size S has a diameter d larger than 5 mm, since having to cover the larger over-all treatment area with a small spot size would be impractical. The thermal relaxation time (TRT) due to the diffusion of heat from a uniformly heated circular

spot of diameter d can be calculated from [30]:

$$TRT_{circle} = d^2/(16 D) \quad , \quad (1)$$

where D is the skin's heat diffusivity ($D \approx 0.1 \text{ mm}^2/\text{s}$). Since the TRT is longer than 15 s for $d \geq 5 \text{ mm}$, the transverse diffusion of heat does not have a significant role in full-spot SMOOTH resurfacing treatments.

For this reason, patterned PS03-type (PS03, PS03X and PS04) handpieces have been developed, where the energy is delivered to the tissue in a "polka dot" pattern, wherein the laser beam irradiates a number (M) of individual spots S within the treatment area S' . Each spot S having the size (e.g., diameter) d is separated from a neighboring spot by the distance x (see Fig. 6).

The spot size d and the distance x are chosen such that the spot size $d \approx 0.8 \text{ mm}$, with $L = 2 \text{ mm}$, and the tissue coverage $TC = (M \times \text{area}(S))/\text{area}(S')$ (in %) is in the range of 25-30%. These parameters ensure that during the time span of the SMOOTH mode pulse (t_{SMOOTH}), the thermal diffusion in the lateral direction spreads the heat generated by laser radiation away from a localized spot S towards the surroundings of the spot, thus effectively spatially homogenizing the slowly varying temperature T_{max} across the area S' . According to Eq. 1, the TRT of the PS03 spots is in the range of 0.4-0.6 s, which is comparable to or shorter than t_{SMOOTH} . Thus, intense heat shocks with short exposure time can be delivered to the localized spots S , without causing long-term overheating of the treatment area S' . In this way it is possible to create an intense heat "needling" on about 30% of the surface of the tissue, whereas the thermal injury in deeper layers is approximately homogeneous (in the lateral direction), since, in the deeper layers, the thermal diffusion spreads the heat in all directions.

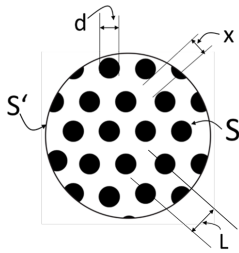


Fig. 6: "Polka dot" spatially patterned delivery of laser pulses with the PS03 or PS03X handpieces.

The influence of the radial heat diffusion for small diameter beams of the PS03 handpiece was investigated in ref [7]. The resulting temporal profiles of soft-tissue surface temperature during a sequence of 4 SMOOTH macro-pulses, delivered by a full-beam (R11 with 7 mm spot size) or by a patterned-beam handpiece (PS03 with

0.85 mm micro spot size) are shown in Fig. 7. As can be seen, with the patterned handpiece, substantially higher temperature peaks (T_{max-i}) were achieved without increasing the final sequence temperature ($T_{max} = 50 \text{ }^\circ\text{C}$).

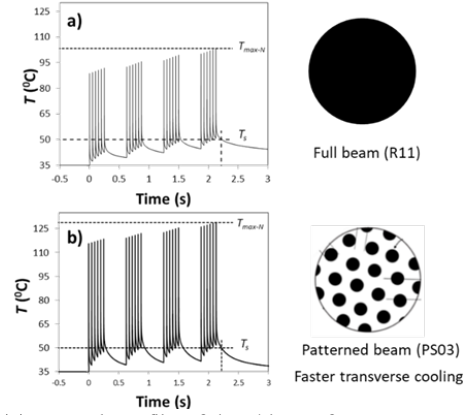


Fig. 7. Temporal profile of the skin surface temperature during a sequence of four SMOOTH mode macro pulses each consisting of six micro pulses (resulting in 24 micro pulses) for (a) $F = 4.9 \text{ J/cm}^2$ with a full-beam handpiece (R11 with 7 mm spot size); and (b) $F_i = 14.7 \text{ J/cm}^2$ with a patterned-beam handpiece (PS03 with 0.85 mm micro spot size) [7].

It is to be noted that maximally the same energy per overall laser spot size can be delivered by both, either a full beam or a patterned handpiece. This is because the maximal temperature $T_{max} = T_s$ (See Fig. 7) which determines the patient's discomfort depends on the overall delivered energy. Therefore, the level of the deep thermal coagulation is not affected by the type of the handpiece. On the other hand, the level of superficial heat-shock triggering which is governed by T_{max-i} is increased significantly within the polka dot spots due to the non-linear dependence of the short-exposure Arrhenius process.

d) Honeycomb beam pattern

A question arises whether a better pattern structure than that used in the PS03x handpiece can be found where a similar coverage TC would be achieved with even faster transverse cooling, and therefore with even more intense heat-shock triggering.

Consider a pattern consisting of rings having the same area as the circles of the standard circular pattern (see Fig. 8). Assuming that the width d of the ring is significantly smaller than its radius r then the TRT of the ring can be calculated from [30]:

$$TRT_{ring} \approx d^2/D \quad (2)$$

A comparison of the TRT s of the two shapes with the same area where the diameter of the circle is equal to $d = 0.8 \text{ mm}$, shows that the TRT of the ring is approximately 2.4-times shorter in comparison with that of the TRT of the circle.

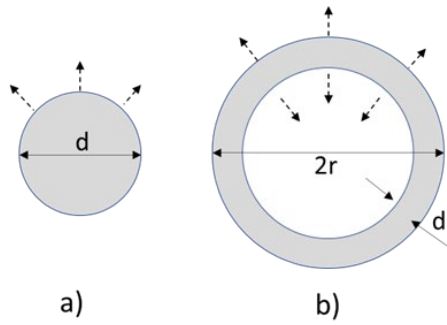


Fig. 8: Example of a circular and a ring pattern with the same surface area S .

An “ideal” patterned coverage of the treated skin surface would be one where the surface is covered by a tessellation, i.e., by a pattern of shapes that fit together without any gaps, and where the laser radiation is present predominantly on the perimeters of the covering shapes. There are only three regular tessellations: those made up of equilateral triangles, squares, or regular hexagons (Fig. 9). Circles or rings cannot cover a surface without gaps which act as an insulation thus reducing the cooling rate of the pattern.

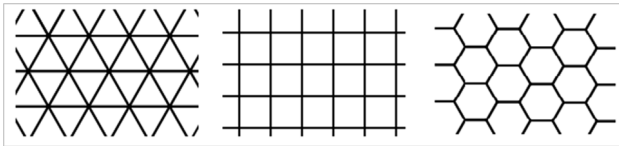


Fig. 9: Three regular tessellations: triangles, squares and hexagons.

Out of these three shapes, the hexagon shape is particularly unique since it is the most efficient way to maximize area while minimizing perimeter [31-38]. As can be seen in Fig. 10, even though the triangle (a) and hexagon (b) have the same perimeter, the latter contains the most triangles (six instead of four).

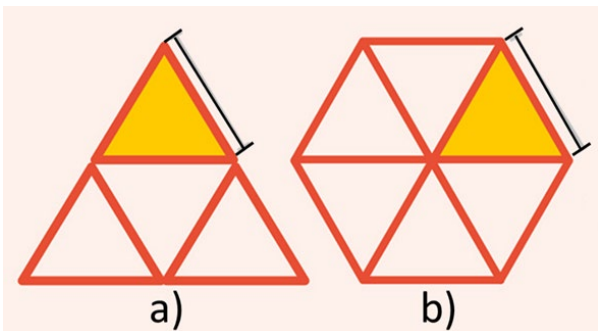


Fig. 10: Example of a triangle (a) and a hexagon (b) having the same perimeter. The hexagon contains more triangles (six instead of four).

It is for this reason that early philosophers have thought that the honeycomb patterns in nature (see Fig. 10) are a result of “heaven-instructed mathematicians” [35].

Therefore, laser heating of the skin along the perimeters of hexagons is expected to result in the shortest thermal relaxation time for the same laser-irradiated surface, since for such pattern the heated hexagons’ perimeters are surrounded by the largest possible non-irradiated surface into which the heated tissue patterns can diffuse the deposited heat.

Based on the above considerations, a special Fotona “HoneyComb™” optics (HC⁶) has been developed, that combines the laser propagation characteristics of the Dynamis laser with the imaging characteristics of the HC⁶ optics. When the HC⁶ optics is installed at the exit of the standard Er:YAG scanner (T-Runner), the standard full-beam pattern of the Fotona T-Runner scanner is transformed into the honeycomb beam pattern (see Fig. 11).



Fig. 11. Fotona HoneyComb HC⁶ optics. By installing the special HC⁶ optics onto the exit of the standard Fotona T-Runner scanner, the previously full-beam output is transformed into a honeycomb-patterned beam.

e) Analysis

An analysis was performed in order to determine the expected difference in the tissue regeneration effect between the full-spot and honeycomb-patterned configuration. The following modeling was applied: i) a numerical model of the physical process of tissue resurfacing, with the details of the physical model and used parameters described in [5, 7, 46]; and ii) an Arrhenius damage integral-based VHS (Variable Heat Shock) chemical model of the tissue response to the short-duration and long-duration thermal exposures, as described in [5, 6, 7, 28].

According to the VHS model the critical temperature for irreversible tissue damage represents a combined effect of two limiting Arrhenius’ processes (see Fig. 12), defining cell viability at extremely long and short exposure times, t [28].

The analysis of the level of superficial triggering (Ω_{HBM}), and of the deep-tissue response represented by the coagulation depth (z_{hyper}) was made for treatments at the patient’s pain tolerance threshold for two FotonaSMOOTH® treatment conditions: without and with topical anesthesia.

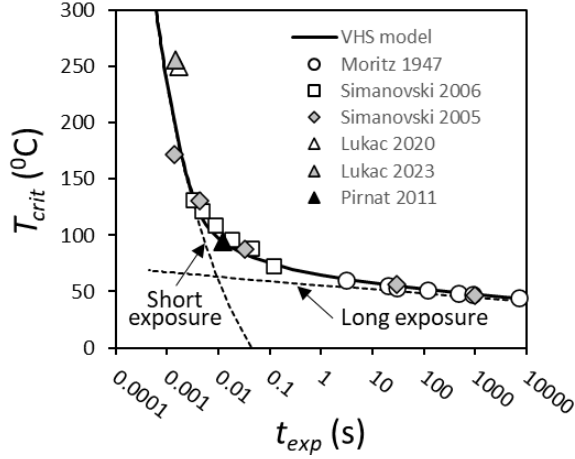


Fig. 12: VHS (Variable Heat Shock) model of tissue response [27,39,40,41,42,45]. For very short thermal exposures the critical temperature is significantly higher than what would be expected from a single Arrhenius' dependence determined for thermal exposures longer than about 1 second.

Pain threshold. As has been shown in ref [7], the pain threshold depends predominantly on T_{max} , with the average pain threshold for different patient populations defined by $T_{max} = T_0 + \Delta T_{max} \approx 48$ °C for the FotonaSMOOTH® treatment without topical anesthesia, and $T_{max} \approx 51$ °C for treatments with topical anesthesia. The study also showed that the final base line temperature growth ΔT_{max} of the treated skin can be estimated by:

$$\Delta T_{max} = \eta \times F, \quad (3)$$

where

$$\eta = A t_{stack}^K. \quad (4)$$

Here, the coefficients for the full beam treatments of cutaneous tissue are $A = 84$ and $K = -0.43$ [66], where the slope η is in units of °C.cm²/J, and the sequence duration t_{stack} is in milliseconds.

Amplitude of short-exposure superficial triggering

(Ω_{i-HBM}). As can be seen from Fig. 13, for extremely short-duration thermal exposures ($t_{exp} < 1$ ms), such as encountered during exposures to high temperature peaks T_{max-i} during Er:YAG smooth-resurfacing (see Fig. 1), the critical temperature is above the soft tissue's threshold temperature of 256 °C required for Er:YAG laser ablation [46]. This means that despite their intensity, the high temperature peaks T_{max-i} are not expected to cause irreversible damage. Instead, they result in superficial heat shocking, representing an additional, indirect (i-HBM) mechanism of action for regenerating epithelial and deeper-lying connective tissues [28, 47-52], which is complementary to the conventional direct slow stimulation of fibroblasts [53].

The amplitude of superficial heat-shock triggering was evaluated by assuming that the level of thermal "needling" is related to the superficial damage resulting from the short-duration exposures, the probability P_i of thermal damage caused by each pulse, $i = 1 \dots N$, calculated from

$$P_i = 1 - \exp(-\Omega_i), \quad (5)$$

where the tissue damage response Ω_i was calculated using a standard Arrhenius rate equation [26-27].

The probability-summation model [54, 55] was used to calculate the cumulative short-exposure Arrhenius process damage to the superficial tissue layer, following a series of $i = 1 \dots N$, intense short-duration thermal exposures to T_{max-i} .

$$P_{i-HBM}(N) = 1 - (1-P_1)(1-P_2) \dots (1-P_N), \quad (6)$$

and the superficial tissue response (Ω_{i-HBM}) was then obtained using Eq. 1, with P_i and (Ω_i) replaced by P_{i-HBM} and Ω_{i-HBM} .

It is to be noted here that although there is a cumulative effect in multiple-pulse exposures [56], the cumulative mechanism may vary depending on the type of tissue and irradiation [55, 56]. Therefore, the short-exposure tissue response Ω_{i-HBM} as calculated using the probability-summation model should be taken merely as an indication of the actual amplitude of heat-shock triggering, and not as the absolute level of the superficial tissue damage.

Long-exposure deep-tissue hyperthermia

/coagulation. The deep-tissue damage integral Ω_{hyper} resulting from the long-duration temperature extending deeper into the tissue (see Fig. 1), is characterized predominantly by the long-pulse exposure process. It was calculated by integrating the damage over temperature instead of over time, using the algorithm developed for calculating tissue damage for temporally non-square-shaped thermal exposure pulses [5, 6, 28]. The coagulation depth ξ_c was obtained as the tissue depth below which the calculated cell injury Ω_{hyper} was smaller than 0.5. Based on the modeling, an approximate formula was found for calculating ξ_c (in μ m), with F expressed in J/cm² and, t_{stack} and τ expressed in ms:

$$\xi_c = F (6.25 + 61.75 \exp(-0.04 t_{stack}/\tau)), \quad (7)$$

where

$$\tau = \exp(0.4 F). \quad (8)$$

III. RESULTS

a) Measurements

Figure 13 shows the hexagonal output beam pattern of the HC⁶ T-Runner as detected on the thermally sensitive paper (Fig. 13a) and measured by a thermal camera (Fig. 13b).

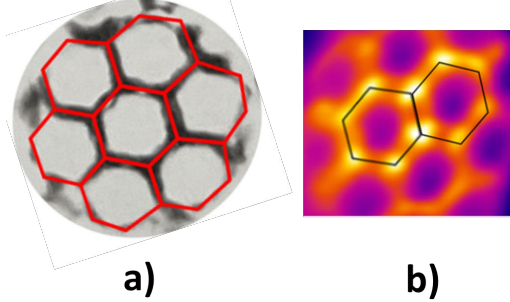


Fig. 13: Hexagonal output beam pattern of the HC⁶-equipped T-Runner scanner, as visible on a thermally sensitive paper (a) and measured by a thermal imaging camera (b).

The measured temporal profiles of the skin surface temperature during a sequence of 6 micro-pulses of a single SMOOTH mode pulse, for the standard (full-beam) T-Runner and for the HC⁶-equipped T-Runner are shown in Fig. 14.

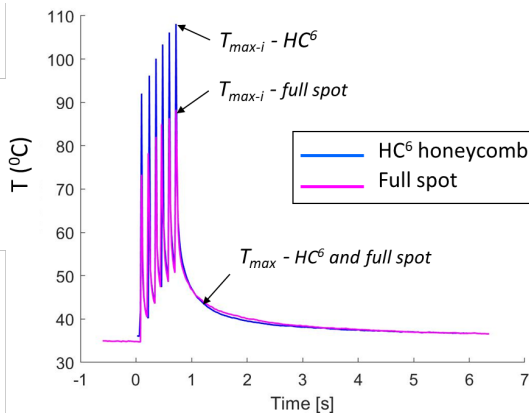


Fig.14: Measured temporal profiles on the treated skin with the full-beam or HC⁶-equipped T-Runner, for the same total laser energy delivered during the 6 micro-pulses of the SMOOTH mode pulse. The distribution of the laser energy into the HC⁶'s honeycomb patterns results in higher peak temperatures T_{max-i} , however, the final temperature T_{max} remains unchanged.

The distribution of the laser energy into the honeycomb patterns results in a higher fluence within the hexagon's perimeters as compared to the top-hat full beam. As can be seen in Fig. 14, this leads to ~ 1.63 -times higher peak temperatures T_{max-i} , however, due to the faster transverse cooling of the hexagonal pattern, the final temperature T_{max} is the same for both T-Runner configurations.

Figure 15 shows temperature profiles for the honeycomb HC⁶ and full-beam configuration, as

measured across a cross section of the treated skin for successive (1-6) micro pulses of the SMOOTH mode pulse.

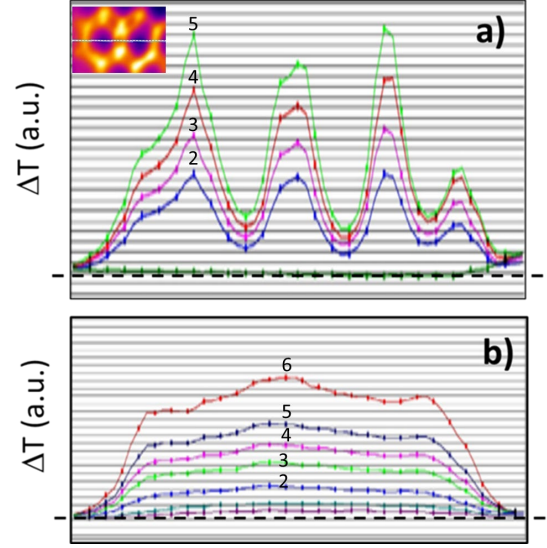


Fig. 15: Temperature profiles for the honeycomb HC⁶ (a) and full spot (b) configuration, as measured across a cross section of the treated skin for successive (1-6) micro pulses of the SMOOTH mode pulse. The same temperature scale applies for both configurations, a) and b).

In detail, Fig. 16 shows normalized temperature profiles immediately after the 5th micro pulse, and at a delay of 100 ms after the 5th micro-pulse. The normalization was performed to compare temperatures for the same energy per overall spotsize applied for both handpiece configurations.

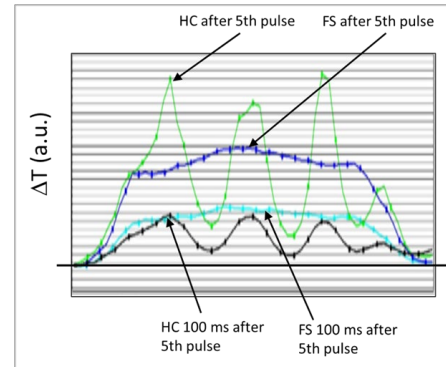


Fig. 16: Normalized temperature profiles for the honeycomb HC⁶ and full-spot (FS) configuration, as measured across a cross section of the treated skin immediately after the 5th micro pulse, and at a delay of 100 ms after the 5th micro-pulse.

b) Analysis

Figure 17 depicts the calculated levels of heat shock triggering (Ω_{i-HBM}) and hyperthermia/coagulation depth (\bar{z}_D) for the FotonaSMOOTH[®] treatment without (Fig. 17a) and with (Fig. 17b) topical anesthesia, as a function of the number (N_{stack}) of delivered SMOOTH mode pulses.

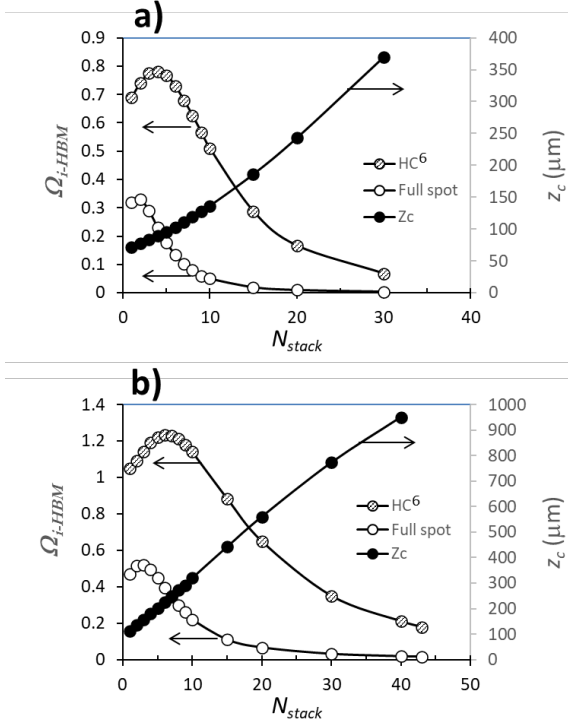


Fig. 17: Amplitude of intense heat shock biomodulation (Ω_{i-HBM}) and coagulation depth (z_c) for the FotonaSMOOTH[®] treatment without (a) and with (b) topical anesthesia, as a function of the number (N_{stack}) of delivered SMOOTH mode pulses. The cumulative fluence F for each N_{stack} train was set to the maximal allowed fluence at which the base-line temperature T_{max} just reaches the pain threshold (see Eqs. 3 and 4).

It is to be noted that increasing the number of laser pulses reduces the superficial triggering effect (Ω_{i-HBM}), since for the same pain threshold, and therefore for approximately the same cumulatively delivered energy, the energies and resulting T_{max-i} of the micropulses must be decreased.

IV. DISCUSSION

The measurements demonstrate that the Fotona Er:YAG T-Runner scanning handpiece, equipped with the special HC⁶ optics, generates a honeycomb-patterned beam pattern (Fig. 14), the pattern that the nature has found to be optimal for covering a surface with the maximal area-to-perimeter ratio. (See Fig. 18)

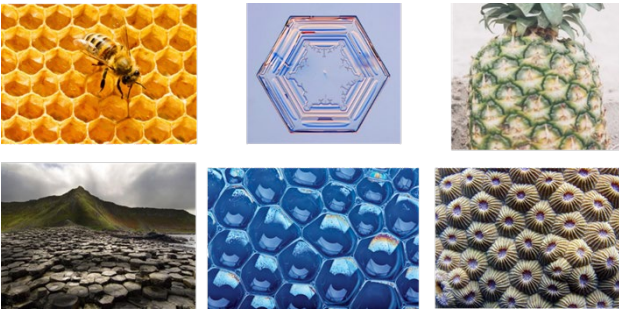


Fig. 18: Examples of honeycomb structures in nature.

The obtained honeycomb pattern leads to an optimal enhancement of the transverse cooling, resulting in a substantial enhancement of the intense heat-shock biomodulation (i.e., superficial triggering), without reducing the deep coagulation/hyperthermia effect.

As can be seen from Fig. 17, while the full-spot temperature ΔT drops by about 42%, the honeycomb temperature drops substantially faster (by 72%) within the same time period. Since for the full-spot illumination the contribution of the transverse heat diffusion is negligible, the observed cooling rate for the full-spot illumination can be attributed mainly to the longitudinal heat diffusion. The 30% difference in the cooling rates is therefore a result of the enhanced transverse heat diffusion of the HC⁶ pattern. This additional cooling rate increase translates into a fast transverse relaxation time of $TRT \approx 0.3$ s, which is sufficiently fast for substantially reducing the base-line temperature build-up during the SMOOTH mode macro pulses.

Without affecting the final base-line temperature (T_{max}) and therefore also not the patients' comfort, the HC⁶ optics enables the generated micro temperature peaks (T_{max-i}) to be higher by a factor of 1.6 in comparison to those achievable by the standard full-spot T-Runner optics. This enhancement translates into an even more substantial enhancement of the i-HBM superficial triggering, by a factor of 2.5 (see Fig. 18).

If the combined regenerating effect (R_{SMOOTH}) of the superficial heat-shock triggering and deep hyperthermia of Fig. 18 is evaluated by a regeneration factor R_{SMOOTH} , where:

$$R_{SMOOTH} = \Omega_{i-HBM} \times z_c \quad (9)$$

where z_c is in μm , then the resulting dependence of the FotonaSMOOTH[®] regeneration effect on N_{stack} is presented in Fig. 19 below.

It is to be noted that although Ω_{i-HBM} and z_c are expressed in different units they represent a typically used measure of the amplitude of the heat shock and coagulation effect, respectively. However, since these two effects are approximately independent of each other, and are expressed in different units, their product, and not for example their sum, was selected as a suitable index.

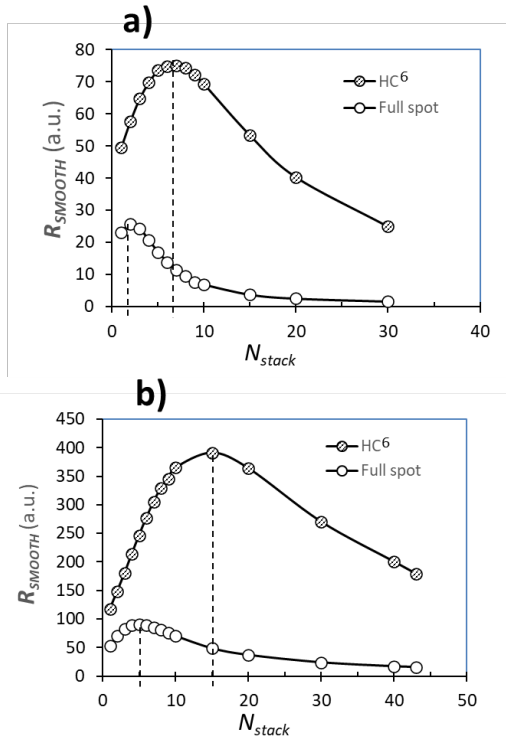


Fig. 19: Dependence of the FotonaSMOOTH® regeneration effect (R_{SMOOTH}), without (a) and with (b) topical anesthesia, as a function of the number (N_{stack}) of delivered SMOOTH mode pulses.

Assuming that the regeneration factor R_{SMOOTH} appropriately describes the synergistic effect of the two FotonaSMOOTH® regeneration mechanisms, then the optimal numbers of SMOOTH mode stacks is $N_{stack} = 2 - 5$ for treatments without, and $N_{stack} = 7 - 15$ for treatments with topical anesthesia.

Finally, Figs. 20 and 21 provide clinical examples of the facial and body treatments performed with the HC⁶-enabled FotonaSMOOTH® laser.



Fig. 20: Facial FotonaSMOOTH® treatment, before (left) and after (right), using the HC⁶-enabled T-Runner Face.



Fig. 21: Abdominal FotonaSMOOTH® treatment, before (left) and after (right), using the HC⁶-enabled T-Runner Body.

IV. CONCLUSIONS

In conclusion, the introduction of the HC⁶ HoneyComb™ technology has enabled optimally patterned large-area FotonaSMOOTH® treatments with the scanning T-Runner handpiece. Without affecting the final base-line temperature (T_{max}), the HC⁶ optics enables the generated micro temperature peaks (T_{max-i}) to be 1.6-times higher in comparison to those achievable by the standard full-spot T-Runner optics. This enhancement translates into an even more substantial enhancement (2.5 x) of the amplitude of intense heat-shock biomodulation (i-HBM).

The HC⁶ patterned-beam Er:YAG laser technology thus represents an important addition to the already widely used patterned PS03-type manual handpiece technology.

REFERENCES

1. Lukac M, Perhavec T, Nemes K, Ahcan A (2010) Ablation and Thermal Depths in VSP Er:YAG Laser Skin Resurfacing. J LA&HA, J Laser and Health academy 2010(1): 56-71.
2. Majaron B, Plestenjak P, Lukac M (1999), Thermo-mechanical laser ablation of soft biological tissue: modeling the micro-explosions. Appl. Phys. B 69, 71–80.

3. Alster TS. Clinical and histologic evaluation of six Erbium:YAG lasers for cutaneous resurfacing. *Lasers Surg Med* 1999; 24:87–92.
4. Khatri KA, Ross V, Grevelink JM (1999) Comparison of Erbium:YAG and Carbon Dioxide Lasers in Resurfacing of Facial Rhytides. *Arch Dermatol* 135(4): 391-397.
5. Lukac M, Zorman A, Bajd F (2018) TightSculpting®: A Complete Minimally Invasive Body Contouring Solution; Part II: Tightening with FotonaSmooth® Technology. *J LA&HA, J Laser and Health Academy*, Vol. 2018, No. 1; 26-35. www.laserandhealth.com
6. Lukac M, Gaspar A, Bajd F (2018) Dual Tissue Regeneration: Non-Ablative Resurfacing of Soft Tissues with FotonaSmooth® Mode Er:YAG Laser. *J LA&HA, J Laser and Health Academy*, Vol. 2018, No. 1; 1-15. www.laserandhealth.com.
7. Lukac M, Zorman A, Lukac N, Perhavec T, Tasic Muc B. Characteristics of Non-Ablative Resurfacing of Soft Tissues by Repetitive Er:YAG Laser Pulse Irradiation. *Lasers Surg Med* 2021;53(9):1266-1278. DOI: 10.1002/lsm.23402
8. Gaspar A, Brandi H, Gomez V, Luque D. Efficacy of Erbium:YAG laser treatment compared to topical estriol treatment for symptoms of genitourinary syndrome of menopause. *Lasers Surg Med [Internet]*. 2016/08/22. 2017 Feb;49(2):160–8.
9. Gaspar A, Brandi H. Non-ablative erbium YAG laser for the treatment of type III stress urinary incontinence (intrinsic sphincter deficiency). *Lasers Med Sci*. 2017;32(3):685–91.
10. Fistončić N, Fistončić I, Guštek ŠF, Turina ISB, Marton I, Vižintin Z, et al. Minimally invasive, non-ablative Er:YAG laser treatment of stress urinary incontinence in women—a pilot study. *Lasers Med Sci*. 2016 May 1;31(4):635–43.
11. Ogrinc UB, Senčar S, Lenasi H. Novel minimally invasive laser treatment of urinary incontinence in women. *Lasers Surg Med [Internet]*. 2015 Nov [cited 2015 Dec 22];47(9):689–97.
12. Bizjak-Ogrinc U, Senčar S. Non-ablative vaginal erbium YAG laser for the treatment of cystocele. *Ital Jounal Gynaecol Obstet [Internet]*. 2017;29(1):19–25.
13. Vizintin Z, Lukac M, Kazic M, Tettamanti M. Erbium laser in gynecology. *Climacteric*. 2015 Oct;18 Suppl 1:4–8.
14. Mitsuyuki M, Štok U, Hreljac I, Yoda K, Vižintin Z, Stok U, et al. Treating Vaginal Laxity Using Nonablative Er:YAG Laser: A Retrospective Case Series of Patients From 2.5 Years of Clinical Practice. *Sex Med*. 2020 Feb;8(2):265–73.
15. Blaganje M, Šćepanović D, Žgur L, Verdenik I, Pajk F, Lukanović A. Non-ablative Er: YAG laser therapy effect on stress urinary incontinence related to quality of life and sexual function: a randomized controlled trial. *Eur J Obstet Gynecol Reprod Biol*. 2018;224:153–8.
16. Kuszka A, Gamper M, Walser C, Kociszewski J, Viereck V. Erbium:YAG laser treatment of female stress urinary incontinence: midterm data. *Int Urogynecol J [Internet]*. 2020;31(9):1859–66.
17. Gambacciani M, Levancini M. Vaginal erbium laser as second-generation thermotherapy for the genitourinary syndrome of menopause: A pilot study in breast cancer survivors. *Menopause*. 2017;24(3):316–9.
18. Storchí IF, Parker S, Bovis F, Benedicenti S, Amaroli A. Outpatient erbium: YAG (2940 nm) laser treatment for snoring: a prospective study on 40 patients. *Lasers Med Sci*. 2018;33(2):399–406.
19. Shiffman HS, Lukac M. NightLase®: minimally invasive laser-assisted uvulopalatoplasty. *J Laser Heal Acad*. 2018;1:39–44.
20. Neruntarat C, Khuancharee K, Shoowit P. Er: YAG laser for snoring: a systemic review and meta-analysis. *Lasers Med Sci*. 2020;35(6):1231–8.
21. Frelich H, Ścierski W, Marków M, Frelich J, Frelich H, Maciej M. Minimally invasive erbium laser treatment for selected snorers. *Lasers Med Sci*. 2019;34(7):1413–20.
22. Picavet VA, Dellian M, Gehrking E, Sauter A, Hasselbacher K. Treatment of snoring using a non-invasive Er: YAG laser with SMOOTH mode (NightLase): a randomized controlled trial. *Eur Arch Oto-Rhino-Laryngology*. 2022;1–6.
23. Ebrahim HM, Gharib K. Correction of nasolabial folds wrinkle using intraoral non-ablative Er: YAG laser Correction of nasolabial folds wrinkle using intraoral non-ablative Er: YAG laser. *J Cosmet Laser Ther*. 2018;00(00):1–5.
24. Gaón NQ, Binfa F. The effect of intraoral 2,940 nm non-ablative Erbium:YAG laser on the rejuvenation of the upper lip: a pilot study. *Surg Cosmet Dermatol*. 2017;9(1):56–8.
25. Matjaz Lukac, Irena Hreljac, Sasa Terlep, Marcelo Tettamanti. “Intense Heat-Shock Biomodulation (i-HBM) of Skin and Mucous Cells with the Fotona SMOOTH® Er:YAG Laser Modality”. *J LA&HA, J Lasers Health Acad* (2022) 2022/1: 1-10.
26. Wright NT (2003) On a relationship between the Arrhenius parameters from thermal damage studies. *Journal of biomechanical engineering* 125(2):300–304.
27. Moritz AR, Henriques FC (1947) Studies of thermal injury, 2. The relative importance of time and surface temperature in the causation of burns. *A J Pathol* 23:695–720
28. Lukac M, Lozar A, Perhavec T, Bajd F. “Variable heat shock response model for medical laser procedures”, *Lasers Med Sci* (2019). <https://doi.org/10.1007/s10103-018-02704-1>
29. Gaspar A, Tettamanti M, Korošec B, Lukač M. Smooth Resurfacing by Hyper Stacking of Er:YAG Laser Pulses; a Histological and Clinical Study. *J Laser Heal Acad*. 2022;1(1):OnlineFirst.
30. Anderson R, Parrish J., The optics of human skin, *J Invest Dermatol*. 1981; 88:13-19.
31. Hepburn, H. R. Honeybees and Wax. An experimental natural history (Springer-Verlag, 1986).
32. Mayr, E. Cause and effect in biology. *Science* 134, 1501 (1961).
33. Pirk, C. W. W., Hepburn, H. R., Radloff, S. E. & Tautz, J. Honeybee combs: construction through a liquid equilibrium process? *Naturwissenschaften* 91, 350–353 (2004).
34. Karihaloo, B. L., Zhang, K. & Wang, J. Honeybee combs: how the circular cells transform into rounded hexagons. *J. R. Soc. Interface*. doi: 10.1098/rsif.2013.0299 (2013).
35. Bartholin, E. De Figura Nivis. *Dissertatio* (Hafniae, 1661).
36. Thompson, D. A. W. *On Growth and Form* (Cambridge University Press, 1917).
37. Ball, P. How honeycombs can build themselves. *Nature*. doi: 10.1038/nature.2013.13398 (2013).
38. Bauer, D. & Bienefeld, K. Hexagonal comb cells of honeybees are not produced via a liquid equilibrium process. *Naturwissenschaften* 100, 45–49 (2013).
39. D. M. Simanovskii, M. A. Mackanos, A. R. Irani, C. E. O’Connell-Rodwell, C. H. Contag, H. A. Schwettman, and D. V. Palanker, Cellular tolerance to pulsed hyperthermia, *Phys Rev E* 74, 011915 (2006), doi: 10.1103/PhysRevE.74.011915.
40. D. Simanovskii, M. Sarkar, A. Irani, C. O’Connell-Rodwell, C. Contag, A. Schwettman, D. Palanker, Cellular tolerance to pulsed heating, *Proc. of SPIE* 5695, 254-259 (2005), doi: 10.1117/12.601774.
41. Lukac N, Tasic Muc B, Lukac M. “High-Temperature Triggering of Soft-Tissue Regeneration by Er:YAG Laser”. *J LA&HA, J Lasers Health Acad* (2020) 2021/1:S3
42. Lukač L, Košir J, Žel T, Kažič M, Šavli D, Jezeršek M. Influence of Tissue Desiccation on Critical Temperature for Thermal Damage during Er:YAG Laser Skin Treatments. *Lasers Surg Med*. (2023)
43. D. M. Simanovskii, M. A. Mackanos, A. R. Irani, C. E. O’Connell-Rodwell, C. H. Contag, H. A. Schwettman, and D. V. Palanker, Cellular tolerance to pulsed hyperthermia, *Phys Rev E* 74, 011915 (2006), doi: 10.1103/PhysRevE.74.011915.
44. D. Simanovskii, M. Sarkar, A. Irani, C. O’Connell-Rodwell, C. Contag, A. Schwettman, D. Palanker, Cellular tolerance to pulsed heating, *Proc. of SPIE* 5695, 254-259 (2005), doi: 10.1117/12.601774.
45. Pirnat S, Lukac M, Ihan A (2011) Thermal tolerance of E. faecalis to pulsed heating in the millisecond range. *Lasers Med Sci* (2011) 26:229–237
46. Majaron B, Plestenjak P, Lukac M (1999), Thermo-mechanical laser ablation of soft biological tissue: modeling the micro-explosions. *Appl. Phys. B* 69:71–80.

47. Hympanova L, Mackova K, El-Domyati M, Vodegel E, Roovers JP, Bosteels J, Krofta L, Deprest J (2020) Effects of non-ablative Er:YAG laser on the skin and the vaginal wall: systematic review of the clinical and experimental literature. *Int Urogynecol J*; <https://doi.org/10.1007/s00192-020-04452-9>
48. Bowman PD. Survival of human epidermal keratinocytes after short-duration high temperature: synthesis of HSP70 and IL-8. *Am J Physiol* 1997; 272(6 Pt 1):C1988-94.
49. Capon A, Mordon S. Can thermal lasers promote skin wound healing?. *Am J Clin Dermatol* 2003; 4 (1): 1-12
50. Mackanosa MA, Contag CH. Pulse duration determines levels of Hsp70 induction in tissues following laser irradiation. *J Biomed Opt* 2011; 16(7), 078002 (July 2011)
51. Lubart R, Friedmann H, Lavie R, Baruchin A . A novel explanation for the healing effect of the Er:YAG laser during skin rejuvenation. *Journal of Cosmetic and Laser Therapy* 2011; 13: 33–34.
52. Manstein D, Scott Herron G, Kehl Sink R, Tanner H, Anderson R. Fractional Photothermolysis: A New Concept for Cutaneous Remodeling Using Microscopic Patterns of Thermal Injury. *Lasers Surg Med* 2004; 34:426–438.
53. Ganceviciene R et al. Skin anti-aging strategies. *Dermatoendocrinol* 2012; 4(3): 308–319.
54. Menendez AR, Cheney FE, Zuclich JA, Crump P. Probability-summation model of multiple laser-exposure effects. *Health Phys* 1993; 65:523–528.
55. Lund BJ, Lund DJ, and Edsall PR. Damage threshold from large retinal size repetitive-pulse laser exposures. *Health Physics* 2014; 107(4):292-299
56. Griess, GA, Blankenstein MF, Williford GG. Ocular damage from multiple-pulse laser exposures. *Health Physics* 198; 39 (Dec):921-927.

The intent of this Laser and Health Academy publication is to facilitate an exchange of information on the views, research results, and clinical experiences within the medical laser community. The contents of this publication are the sole responsibility of the authors and may not in any circumstances be regarded as official product information by medical equipment manufacturers. When in doubt, please check with the manufacturers about whether a specific product or application has been approved or cleared to be marketed and sold in your country.